Two Different Charge Separation Pathways in Photosystem II[†]

Elisabet Romero,*,[‡] Ivo H. M. van Stokkum,[‡] Vladimir I. Novoderezhkin,[§] Jan P. Dekker,[‡] and
Rienk van Grondelle[‡]

[‡]*Department of Physics and Astronomy, Faculty of Sciences, VU University Amsterdam, De Boelelaan 1081,
1081 HV Amsterdam, The Netherlands, and* [§]*A. N. Belozersky Institute of Physico-Chemical Biology,
Moscow State University, Leninsky Gory, 119992 Moscow, Russia*

ABSTRACT: Charge separation is an essential step in the conversion of solar energy into chemical energy in photosynthesis. To investigate this process, we performed transient absorption experiments at 77 K with various excitation conditions on the isolated Photosystem II reaction center preparations from spinach. The results have been analyzed by global and target analysis and demonstrate that at least two different excited states, $(Chl_{D1}Phe_{D1})^*$ and $(P_{D1}P_{D2}Chl_{D1})^*$, give rise to two different pathways for ultrafast charge separation. We propose that the disorder produced by slow protein motions causes energetic differentiation among reaction center complexes, leading to different charge separation pathways. Because of the low temperature, two excitation energy trap states are also present, generating charge-separated states on long time scales. We conclude that these slow trap states are the same as the excited states that lead to ultrafast charge separation, indicating that at 77 K charge separation can be either activation-less and fast or activated and slow.

Charge separation is one of the key processes in photosynthetic energy conversion. After absorption of a photon by the photochemically active reaction center, an electronically excited state is transformed into a short-lived charge-separated state. Subsequent electron transfer results in a stable charge-separated state which ultimately powers the photosynthetic organism.

Type II reaction centers found in purple bacteria and in oxygen-evolving organisms (cyanobacteria, algae, and higher plants) are membrane proteins that contain four (bacterio)chlorophyll [(B)Chl][1] and two (bacterio)pheophytin [(B)Phe] molecules arranged in two symmetric branches spanning the membrane in the center of the complex. It is established that only one branch is active in charge separation (*1*–*4*).

The best understanding of the kinetics and energetics of charge separation has been obtained for the reaction center (RC) of photosynthetic purple bacteria (*5*). The central excitonically coupled special pair, P, of BChl molecules [P_A and P_B, ~8 Å apart, center to center (*6*)], absorbing at ~875 nm in *Rhodobacter sphaeroides*, are electronically excited after the energy transfer from the LH1 core antenna (absorbing at approximately equal energy). Then, an electron is transferred to the BChl molecule on the active branch (B_A) in 3 ps, and from B_A to the BPhe (H_A) in 1 ps, resulting in the final charge-separated state, $P^+H_A^-$. However, in isolated reaction centers, excitation of the accessory BChl absorbing at ~800 nm (B_A) resulted in an even faster charge separation, either via $B_A^+H_A^-$ or via $P^+B_A^-$ (*7*–*9*). In vivo, this second route does not occur to a significant extent, because B_A is too high in energy to receive excitation energy from the antenna.

In the photosystem II reaction center (PSII RC) of oxygen-evolving organisms, there is no special pair, and the similar distance of ~10–11 Å between neighboring pigments in the center of the complex (*10*–*13*) gives rise to a system of coupled pigments (*14*, *15*) that interact, creating collective excited (or exciton) states with contributions from several pigments.

The PSII RC, the unique molecular machinery capable of using light to create a charge-separated state that drives water splitting, contains four chlorophyll and two pheophytin molecules (Phe_{D1}, Chl_{D1}, P_{D1}, P_{D2}, Chl_{D2}, and Phe_{D2}, the RC core), two additional chlorophyll molecules ($Chls_z$), located at opposing sites on the periphery of the complex ~25 Å from the core pigments, and two β-carotene molecules located between $Chls_z$ and the RC core (*10*–*13*). The system is continuously moving: fast nuclear motions (intra- and interpigment vibrations and protein vibrations) and slow conformational motions of the protein produce homogeneous and inhomogeneous broadening, respectively, of the electronic transitions. The low-energy side of the spectra, the Q_y region, is characterized by ultrafast energy equilibration among the cofactors in the RC core, radical pair (RP) formation, and excitation energy transfer from $Chls_z$ to the RC core. The superposition of these processes greatly complicates the interpretation of the transient absorption data and has led to a long and extensive debate in the literature regarding the mechanism and time scale of charge separation (*15*, *16*).

Recent work (*17*, *18*) at room temperature indicates that the charge separation process follows the sequence RC* → $Chl_{D1}^+Phe_{D1}^-$ → $P_{D1}^+Phe_{D1}^-$ → $(P_{D1}^+Phe_{D1}^-)_{relaxed}$. In ref *18*, an additional Chl_z excited state, Chl_z^*, which feeds excitation energy into the RC core was included.

Previously, we have described all the available PSII RC spectroscopic data at room and low temperature within a physical model that takes into account the coupling of excitations to fast and

*To whom correspondence should be addressed. E-mail: eli@few.vu.nl. Telephone: 0031-(0) 20 59 87426. Fax: 0031-(0) 20 59 87999.
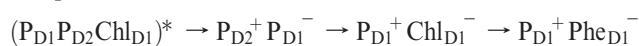[1]Abbreviations: BChl, bacteriochlorophyll; BPhe, bacteriopheophytin; Chl, chlorophyll; Phe, pheophytin; PSII RC, photosystem II reaction center; RP, radical pair; CT, charge transfer; fwhm, full width at half-maximum; λ_{exc}, excitation wavelength; OD, optical density; DADS, decay-associated difference spectra; EADS, evolution-associated difference spectra; SADS, species-associated difference spectra; SE, stimulated emission; FLN, fluorescence line narrowing.

slow motions of the system (*19*). In this model, the excited-state manifold includes a primary charge transfer (CT) state that is strongly mixed with the exciton states. Such a mixing connects the lowest exciton state with the CT state; i.e., it facilitates the formation of the first radical pair. The lowest exciton state is a multimeric state (*14, 20*), a coherent superposition of several PSII RC core pigments, the contribution of each pigment being not uniform and strongly dependent on protein conformation (static disorder) (*19*). Therefore, for the lowest exciton state, several combinations with different participation of different pigments are possible, which can lead to different charge separation pathways. The best description of the available data was obtained for the charge separation pathways:

Chl_{D1} path :

$$(Chl_{D1}Phe_{D1})^* \rightarrow Chl_{D1}^+ Phe_{D1}^- \rightarrow P_{D1}^+ Phe_{D1}^-$$

P_{D1} path :

$$(P_{D1}P_{D2}Chl_{D1})^* \rightarrow P_{D2}^+ P_{D1}^- \rightarrow P_{D1}^+ Chl_{D1}^- \rightarrow P_{D1}^+ Phe_{D1}^-$$

(note that in this representation the cofactor sequence reflects the order of participation in the excitonic wave function).

In this study, we analyzed the energy transfer and charge separation reactions in the isolated PSII RC by transient absorption spectroscopy in much greater detail than was done previously. We simultaneously probed a large spectral range (from 425 to 730 nm, to investigate not only the Q_y region of Chl and Phe but also the Phe Q_x band at 544 nm and the Phe anion band at ∼455 nm), monitored an extensive time range (from 10 ps before to 3 ns after the excitation pulse, to investigate all various time scales of charge separation), recorded the data at 77 K (to enhance the spectral resolution and reduce back reactions and uphill energy transfer), and used various excitation conditions (to allow photoselection of subpopulations with different proportions of Chl_{D1} and P_{D1} pathways). Combining all results and using global and target analysis according to a kinetic scheme, we demonstrate that, in agreement with the theoretical model (*19*), at least two different charge separation pathways are operational in the isolated PSII RC. In addition, we identify two long-lived trap states that form the final radical pair on a long time scale, indicating that both initial excited states give rise to their own spectrally and kinetically distinguishable trap state at 77 K.

MATERIALS AND METHODS

Sample Preparation. The PSII RC (D1−D2−cyt b_{559}) complexes were isolated from spinach as described in ref *21*. The sample was diluted in a buffer containing 60% glycerol (v/v), 20 mM BisTris (pH 6.5), 200 mM sucrose, and 0.06% β-DM. The optical density of the sample was ∼1 mm^{-1} at 678 nm.

Laser System. The seed pulse from a diode-pumped oscillator (Coherent Vitesse, 800 nm, 80 MHz) was amplified to 2.5 W by using a Nd:YLF high-power pump laser (Coherent Evolution-20, 527 nm). The Ti:sapphire-based amplifier (Coherent Legend-UHP) incorporates chirped pulse amplification (CPA) to deliver sub-50 fs pulses, with a center wavelength of 800 nm and 15 nm full width at half maximum (fwhm). The probe pulse, a white light continuum, was generated by focusing a small fraction of the fundamental 800 nm pulses into a laterally rotating CaF_2 plate. The duration of the white light pulses was ≈120 fs because of group velocity dispersion introduced by the medium. The tunable pump pulses were generated by a commercial optical paramagnetic amplifier (OPA, Coherent OperA) pumped by the

Legend-UHP. The pump pulse duration was ≈100 fs with 10 nm fwhm. To generate the transient absorption data, we modulated the pump at 166.5 Hz. The polarization between pump and probe pulses was set to magic angle (54.7°). The pump and probe pulses were focused on the sample with spot sizes 160 and 75 μm in diameter, respectively. After the sample, the probe was spectrally dispersed by a 15 cm focal length spectrograph (Oriel) equipped with a 300 lines/mm and 500 nm blazed grating onto a home-built 256-pixel photodiode array. The temporal and spectral resolution were ≈140 fs and ≈1 nm, respectively.

Experimental Design. Femtosecond transient absorption spectra were recorded at 77 K in the visible range from 425 to 730 nm. To avoid singlet−triplet annihilation and sample degradation due to the accumulation of triplet states (lifetime of 1−2 ms), the laser system was operating at a repetition rate of 333 Hz (i.e., 6 ms between pump pulses). Six narrow (5 nm fwhm) excitation wavelengths (λ_{exc}) were used: 660, 665, 670, 675, 680, and 685 nm. In addition, three broader excitations (fwhm) were used: 662 nm (8 nm), 675 nm (12 nm), and 682 nm (8 nm). The excitation power was sufficiently low to avoid multiple excitations in a single reaction center complex (5.5−30 nJ/pulse depending on λ_{exc}). The absence of annihilation was checked by power dependence series of measurements. Typically, nine scans were recorded and averaged per data set. Each scan consisted of 275 time delays from −10 ps to 3 ns (225 time points from −10 to 100 ps), with 1000 shots taken and averaged per time delay. Statistics in real time were performed. The data was accepted only when 50% of the 1000 shots taken for time delay were within a standard deviation of 5%. Otherwise the data was discarded until it satisfied the statistical restrictions. We checked the sample integrity before and after the measurement by recording the steady-state absorption spectrum. After measurement for the usual 5 h, no sample degradation was observed.

Data Analysis. Global analysis using both parallel decaying and sequential models was applied to all data sets individually. Target analysis was performed on different groups of linked data sets as well as on individual data sets. The results were consistent.

RESULTS

Low-temperature (77 K) transient absorption spectra of the isolated PSII RC from spinach have been recorded for different sets of excitation wavelengths: six narrow excitation wavelengths at 660, 665, 670, 675, 680, and 685 nm (5 nm fwhm) (Figure 1); two broader excitation wavelengths at 662 and 682 nm (8 nm fwhm); and a nonselective excitation wavelength at 675 nm (12 nm fwhm) (Figure S1 of the Supporting Information). The first step in this study is the application of global analysis (*22*) using both a parallel decaying and a sequential model to follow the spectral evolution in time. The second step is to test the presence of multiple charge separation pathways by target analysis (*22*).

The interpretation of the spectra obtained after global and target analysis in the spectrally congested Q_y region is based on the known cofactor absorption: the peripheral $Chls_z$ absorb at 670 nm (*23−25*), both Phe_{D2} and Phe_{D1} absorb at 680 nm (*26*), Chl_{D1} and Chl_{D2} also contribute to the 680 nm spectral region (*27−31*), and P_{D1} is centered at 672.5 nm (*27*).

An essential aspect of this study is the analysis of the spectrally isolated Phe Q_x band at 544 nm. The time-dependent background in this region is minimized by setting ΔA_{557} equal to 0 (*32, 33*) which facilitates the visualization of the bleach dynamics. The Phe Q_x bleach around 544 nm is present when Phe is either excited or reduced, and the Phe anion absorption band at around

455 nm occurs only when Phe is reduced, i.e., participating in a radical pair.

Global Analysis. To identify the spectral components present in the system and estimate their lifetimes, a global analysis was performed on all the data sets using a parallel model with exponential decays. The resulting decay-associated difference spectra (DADS) and their lifetimes are given in Figure S2 and Table S1 of the Supporting Information. However, since it is
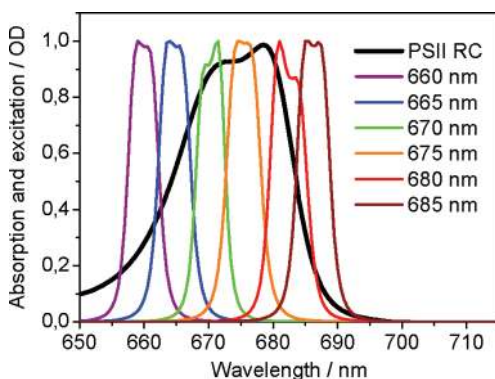
generally accepted that the dynamics in the PSII RC follow the excited state $(RC^*) \rightarrow RP1 \rightarrow RP2$ sequence, a sequential model in which one component decays into the next one is more appropriate. On the basis of the estimated lifetimes (Table S1), we chose six components with common lifetimes of 500 fs, 3 ps, 20 ps, 300 ps, 600 ps, and 20 ns to fit all the data and to facilitate comparison among the different data sets. The obtained evolution-associated difference spectra (EADS) represent a mix of species whose populations rise with the lifetime of the previous component and decay with their lifetimes. For instance, the 20 ps EADS rises in 3 ps and decays in 20 ps (*22*).

The EADS for narrow excitation are shown in Figure 2. In the Q_y region, the initial bleach contains all initially populated exciton states and the Chls$_z$ excited states, the proportion of which depends on the excitation wavelength. The signal after 500 fs is the combination of the absorbance changes caused by the disappearance of the lowest exciton states of the RC core, Chls$_z$ excited states that only transfer excitation energy to the RC core on the 20 ps time scale (*23, 34, 35*), and the appearance of the first radical pair(s).

At first sight, the spectral evolution in the Q_y region can be divided into two groups with two main characteristics: blue excitation (660−670 nm) with up to 20 ps two main bleaches at around 670 and 680 nm with the amplitude of the 680 nm bleach increasing from 500 fs to 300 ps and red excitation (680−685 nm)
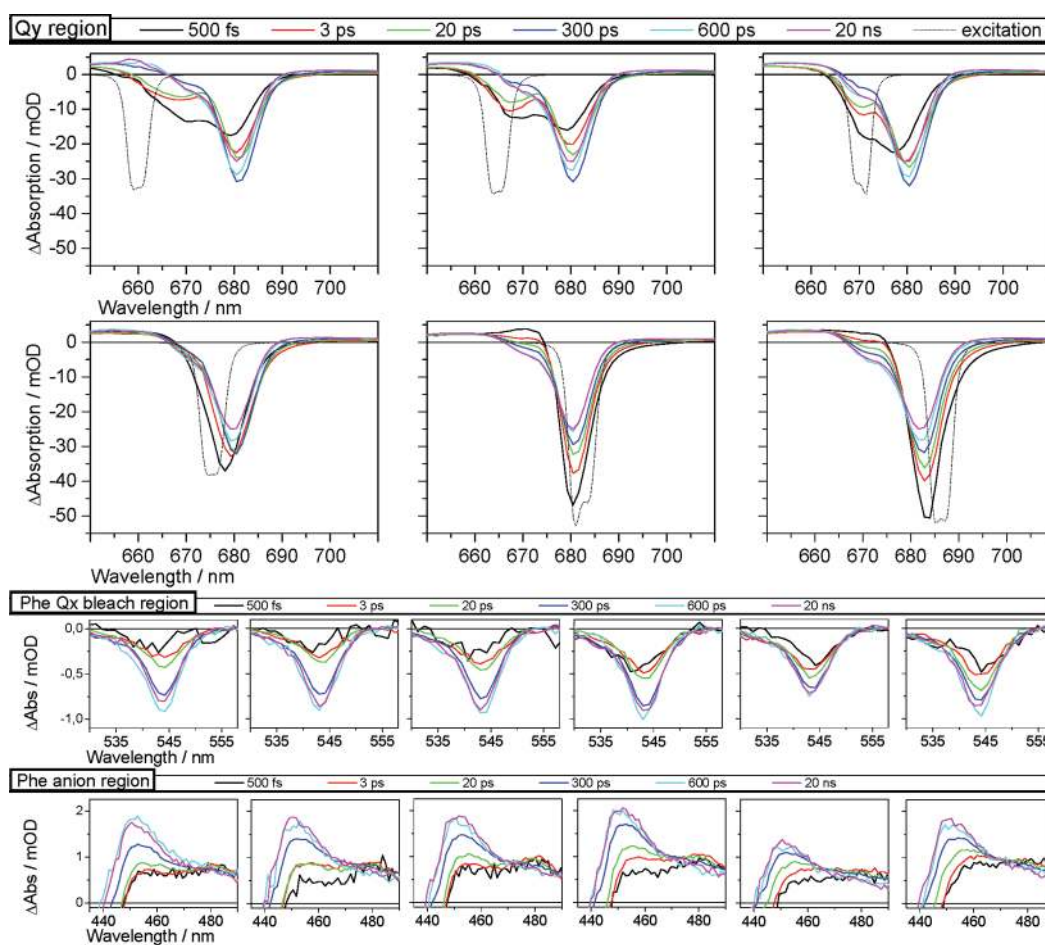

FIGURE 1: Photosystem II reaction center (PSII RC) absorption spectrum at 77 K (thick line) and narrow laser excitation profiles (thin lines).

FIGURE 2: Evolution-associated difference spectra (EADS) for narrow excitations. The top six panels show the Q_y absorption region (from top to bottom and from left to right) for 660, 665, 670, 675, 680, and 685 nm excitation. The middle panels show the Phe Qx absorption region after background subtraction (from left to right) for 660−685 nm excitation. The bottom panels show the Phe anion absorption region (from left to right) for 660−685 nm excitation. Solid colored lines are EADS, and dotted black lines are inverted laser excitation profiles. The EADS have been normalized to the long-lived component (20 ns).

with one main bleach at around 680 nm decreasing in amplitude from 500 fs to 20 ns and a shoulder around 672 nm developing from 3 to 600 ps (675 nm excitation being an intermediate case between blue and red excitation). The final evolution, from 300 to 600 ps and from 600 ps to 20 ns, is very similar for all excitations, indicating that on this long time scale the system evolves to a common species independent of the excitation wavelength. After 600 ps, the similarity between the spectra of the 600 ps and 20 ns components suggests the relaxation of the final RP, $P_{D1}{}^{+}Phe_{D1}{}^{-}$.

(*i*) *Red Excitation* (*680−685 nm*). The 500 fs component is dominated by a single bleach at 680.5 and 681.5 nm for 680 and 685 nm excitation, respectively (Figure 2), in agreement with the population of exciton states containing at least Chl_{D1}, Chl_{D2}, Phe_{D1}, and/or Phe_{D2} (*26−29, 31*) and the stimulated emission (SE) from these excited states at the red side of the bleach. It is worth noting that the Q_y position for the long-lived state shifts to the red upon increasing the excitation wavelength, which implies that photoselection of subpopulations from the inhomogeneous distribution has been achieved. After 500 fs, the main 680 nm bleach decreases and a shoulder around 672 nm appears. After 3 ps, a further 680 nm bleach decrease and a 672 nm bleach increase are observed. A similar evolution is observed from 3 to 20 ps, from 20 to 300 ps, and from 300 to 600 ps. The spectral properties of this evolution are in agreement with the disappearance of an excited state/RP-containing Chl_{D1} and the appearance of a RP-containing P_{D1}: $Chl_{D1}*/Chl_{D1}{}^{+}Phe_{D1}{}^{-}$ (RP1) → $P_{D1}{}^{+}Phe_{D1}{}^{-}$ (RP2). The RP1 → RP2 evolution should give rise to a fully bleached Phe Q_x band in the 3 ps component that will remain constant in the subsequent EADS (*18*). However, the spectral evolution of the Phe Q_x band at 544 nm shows a different behavior (Figure 2 and Table S2 of the Supporting Information). The amplitude of the bleach increases over a range of time scales: 500 fs (mainly due to Phe*) and 3, 20, and 300 ps (mainly due to the formation of $Phe_{D1}{}^{-}$). The evolution in the Phe_{D1} anion band at 455 nm is in agreement with the slow phases (20 and 300 ps) of RP formation containing Phe_{D1}. The slower phases of $Phe_{D1}{}^{-}$ formation were previously observed (at room and low temperature) but were interpreted as charge separation limited by slow energy transfer from a red Chl_z (*18, 32, 36*). We will show (see below) that the $Chls_z*$ are not populated upon 680−685 nm excitation, which excludes the possibility that the slow charge separation upon red excitation is caused by the energy transfer from $Chls_z$ to the RC core. The slow phases of $Phe_{D1}{}^{-}$ formation indicate that the Chl_{D1} path as a unique charge separation mechanism (*17, 18*) is not able to explain the observed dynamics.

(*ii*) *Blue Excitation* (*660−670 nm*). The spectral shape of the 500 fs component (Figure 2) is highly dependent on excitation wavelength. However, two common bleaches at 670 and 679 nm are observed for blue excitation. The 670 nm bleach corresponds to the $Chls_z$ excited state (*23*) and exciton states containing P_{D1} (*27*) and higher exciton states. The 679 nm bleach reflects the population of an exciton(s) with participation of at least Chl_{D1}, Chl_{D2}, Phe_{D1}, and/or Phe_{D2} (*26−29, 31*). The main changes from the 500 fs to the 3 ps component are the decrease in the 670 nm bleach and the increase and red shift of the 680 nm bleach. This evolution can be explained by exciton relaxation from the levels near 670 nm to the lowest levels peaking near 680 nm. After 3 ps (20 ps EADS), a further 670 nm bleach decrease and a 680 nm bleach increase are observed. After 20 ps, the 670 nm bleach disappears and a substantial increase in the 680 nm bleach is

observed, indicating that the energy transfer from $Chls_z$ to the RC core is completed (*23, 34, 35*). The shoulder at ∼672 nm reflects the formation of a RP-containing P_{D1} (*27*). After 300 ps, the 600 ps component appears with a further increase in the 672 nm shoulder and a decrease in the 680 nm bleach. The spectral evolution is in agreement with the Chl_{D1} path: $Chl_{D1}{}^{+}Phe_{D1}{}^{-}$ (RP1) → $P_{D1}{}^{+}Phe_{D1}{}^{-}$ (RP2). However, on a long time scale, after 300 ps, a Phe Q_x bleach increase of 15−20% is again observed. The slow phases (20 and 300 ps) of RP formation containing Phe_{D1} are confirmed by the evolution in the Phe_{D1} anion band at 455 nm (Figure 2).

(*iii*) *$Chls_z*$ Population and Energy Transfer to the RC Core Pigments*. The evolution of the $Chls_z*$ population can be indirectly estimated by quantifying the amount of excitation energy present in the RC core at a certain time after excitation. The energy located in the RC core is measured as the amplitude of the Phe Q_x bleach for each component with respect to the final total amplitude (600 ps component). When blue and red excitations are compared on the long time scale, 300 ps, the Phe Q_x bleach amplitude is very similar. However, on the short time scale, it is clear that for blue excitation the initial amount of excitation energy in the RC core is lower: ∼29% for the 500 fs component versus ∼52% for red excitation. This significant difference indicates that for blue excitations part of the excitation energy is absorbed by cofactors not located in the RC core. Another significant difference is the Q_x bleach amplitude increase after 20 ps: ∼34% for blue and ∼13% for red excitation (last column in Table S2 of the Supporting Information), indicating that for blue excitation after 20 ps a significant amount of energy has been delivered to the RC core (apart from the Phe Q_x bleach increase due to RP formation). These observations are in agreement with both $Chls_z$ absorbing around 670 nm and with the 20 ps lifetime for the energy transfer from $Chls_z$ to the RC core (*23, 34, 35*). Therefore, we can confidently conclude that (i) $Chls_z$ are not populated with 680−685 nm excitation and (ii) the energy transfer from $Chls_z$ to the RC core occurs with a lifetime of 20 ps, not on longer time scales (*18, 32, 36*).

Target Analysis. The results from the global analysis strongly indicate that the generally accepted charge separation process described by the Chl_{D1} path is not unique. Therefore, additional channels of charge separation must be operational in the PSII RC. To test this hypothesis, we perform a target analysis.

The kinetic scheme that serves as the input for the target analysis consists of two parallel charge separation pathways, Chl_{D1} and P_{D1} paths, each with compartments representing the excited states and the first radical pair (RP1) converging to a common secondary radical pair (RP2) that relaxes on the long time scale, with two additional compartments, $Chl_{z667}*$ and $Chl_{z670}*$, which transfer excitation energy to the RC core slowly (Figure 3). To gather sufficient information to resolve the spectra of eight compartments with the complication of two parallel processes occurring on the same time scale, we analyzed several data sets simultaneously. Six data sets [660, 665, 670, and 675 nm (5 nm fwhm); 662 nm (8 nm fwhm); and 675 nm (12 nm fwhm)] have been linked in the target analysis. The 680, 682, and 685 nm excitations are not included because of the strong photoselection which produces an up to 2 nm red-shifted final state with respect to blue excitation that impedes the simultaneous analysis of the whole collection of data sets (Figure 2). The target analysis results in estimated species-associated difference spectra (SADS) and microscopic decay rates. The SADS are in a first approximation the pure spectra of the species represented by the kinetic
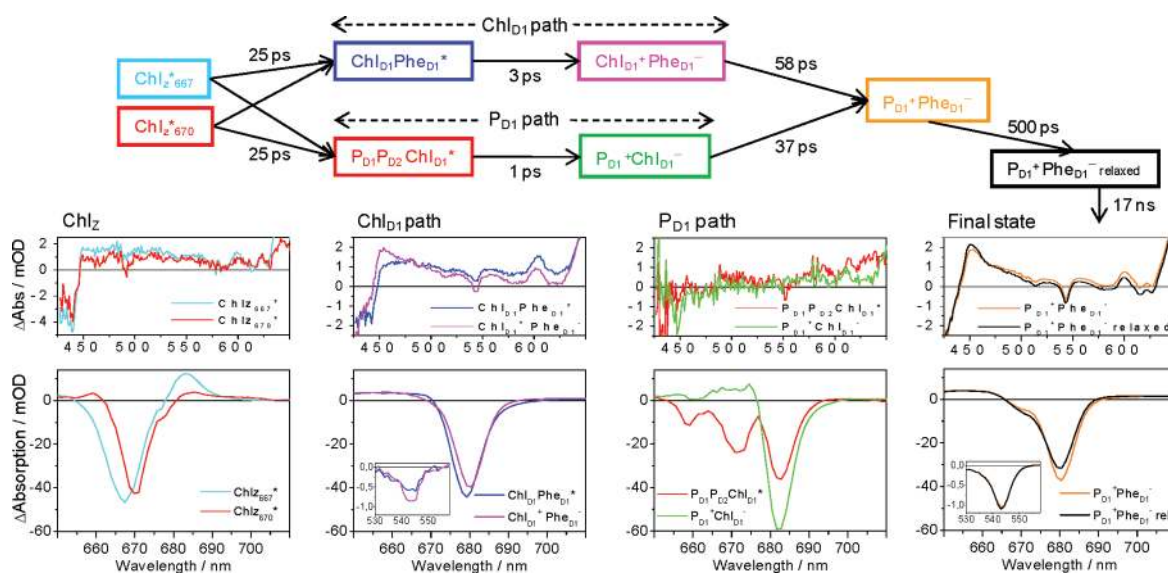
FIGURE 3: Kinetic scheme with two parallel charge separation pathways (top). SADS corresponding to the kinetic compartments (bottom). Insets show the Phe Q_x bleach after background subtraction. The equivalent graphs are plotted on the same scale for better comparison (except for the 425−650 nm region for Chls$_z$).

compartments (the uncertainty arises due to the spectral congestion and due to the fact that all processes occur almost simultaneously). The kinetic scheme, rate constants, and SADS are shown in Figure 3. The target analysis also estimates the initial proportion of RCs following each pathway and the contribution of Chls$_z$ to the total absorbed energy for the different subpopulation photoselected by each excitation wavelength (Table S3 of the Supporting Information).

(*i*) *Chls$_z$*. Due to photoselection, two SADS are obtained for Chls$_z$ with bleaches centered at 667 and 670 nm, SE around 675 and 677 nm, and a positive band at 685 nm assigned to excited-state absorption. The rate of energy transfer from both Chls$_z$* to the RC core is $1/25$ ps^{-1}, in agreement with the 20 ps lifetime for Chls$_z$* obtained from the global analysis and the literature (*23, 34, 35*).

(*ii*) *Chl$_{D1}$ Path*. In the Q_y region, the RC* SADS (Chl$_{D1}$Phe$_{D1}$)* consists of a bleach centered at 679 nm. This state decays in 3 ps to form a RP1 (Chl$_{D1}$+Phe$_{D1}$−) whose SADS is 1 nm red-shifted. Both SADS contain the Phe Q_x bleach at 544 nm, while RP1 shows a clear Phe anion band at 455 nm. The Phe features indicate that Phe is involved in this pathway, and the Q_y bleach at 679 nm suggests the involvement of Chl$_{D1}$, in agreement with the (Chl$_{D1}$Phe$_{D1}$)* → Chl$_{D1}$+Phe$_{D1}$− transition. This assignment, excited state and RP, is also based on the presence of SE around 690 nm in the former and the typical RP-induced absorption in the 700−730 nm region in the latter.

(*iii*) *P$_{D1}$ Path*. In the Q_y region, the RC* SADS (P$_{D1}$P$_{D2}$Chl$_{D1}$)* contains bleaches at 660, 667, and 680 nm with relative amplitudes of 0.3, 0.7, and 1, respectively. The absence of the Phe features in both the RC* and RP1 (P$_{D1}$+Chl$_{D1}$−) spectra implies that Phe does not play a role in these states. Therefore, the bleaches at 660, 667, and 680 nm are consistent with contribution from high exciton states, P$_{D1}$ and/or P$_{D2}$, and Chl$_{D1}$, respectively, in agreement with the (P$_{D1}$P$_{D2}$Chl$_{D1}$)* → P$_{D2}$+P$_{D1}$− → P$_{D1}$+Chl$_{D1}$− process. The RP1 spectrum has a significant bleach at 682 nm (suggesting the involvement of Chl$_{D1}$) but lacks the negative signal at 670 nm expected for oxidation of P$_{D1}$. It should be noted that the interpretation of the RP spectra is not straightforward, because oxidation or reduction will likely

lead to electrochromic shifts of the absorbance spectra of nearby cofactors.

(*iv*) *Secondary Electron Transfer*. Then, both pathways converge by the transfer of an electron from Chl$_{D1}$− to Phe$_{D1}$ with a rate constant of 0.027 ps^{-1} (Chl$_{D1}$ path) and from P$_{D1}$ to Chl$_{D1}$+ with a rate constant of 0.017 ps^{-1} (P$_{D1}$ path). The RP2, P$_{D1}$+Phe$_{D1}$−, SADS is well-known in the literature with a main 680 nm bleach (Phe$_{D1}$), a shoulder around 672 nm (P$_{D1}$), a Phe Q_x band bleach, and a Phe anion absorption band. Compared to the final SADS, some additional excited-state absorption appears to be present between 475 and 625 nm.

(*v*) *"Relaxation" Process*. Surprisingly, in contrast with the initially hypothesized relaxation process, the spectral evolution on the 500 ps time scale shows a further increase in the population of the P$_{D1}$+Phe$_{D1}$− final state: in the Q_y region, there is an increase in the 672 nm shoulder and a decrease in the 680 nm bleach, and the amplitude of the Phe anion band suggests an increase in the Phe$_{D1}$− population of around 20%. These findings point to the existence of a very slow channel of charge separation, which was also observed in the global analysis. It is interesting to note that from the global analysis the increase in the Phe$_{D1}$− population on the long time scale was also around 20%. The fact that a 20% increase in the Phe anion band but a very small increase of less than 5% in the Phe Q_x band are observed indicates that a Phe excited state is transformed into Phe$_{D1}$−.

Simplified Target Analysis. The inclusion of an extra compartment in the kinetic scheme is not possible with the available data. For this reason, we have applied a simplified target analysis in which the two parallel pathways are condensed in two compartments (RC* and RP1). This allows us to include the slow phase of charge separation observed in the data.

The kinetic scheme that gives the best fit to the data consists of four excited states (Chls$_z$*, RC*, Trap$_{65}$*, and Trap$_{585}$*) and two radical pairs [one containing a mix of RP1s and the other corresponding to the final charge-separated state, P$_{D1}$+Phe$_{D1}$− (RP2)] (Figure 4). After 17 ps, the Chls$_z$ excitation energy is transferred to the RC core. Trap$_{65}$* is depopulated in 65 ps to form RP2. Features of this process were already present in the DADS at 46, 39, and 36 ps (for 665, 680, and 685 nm excitation,
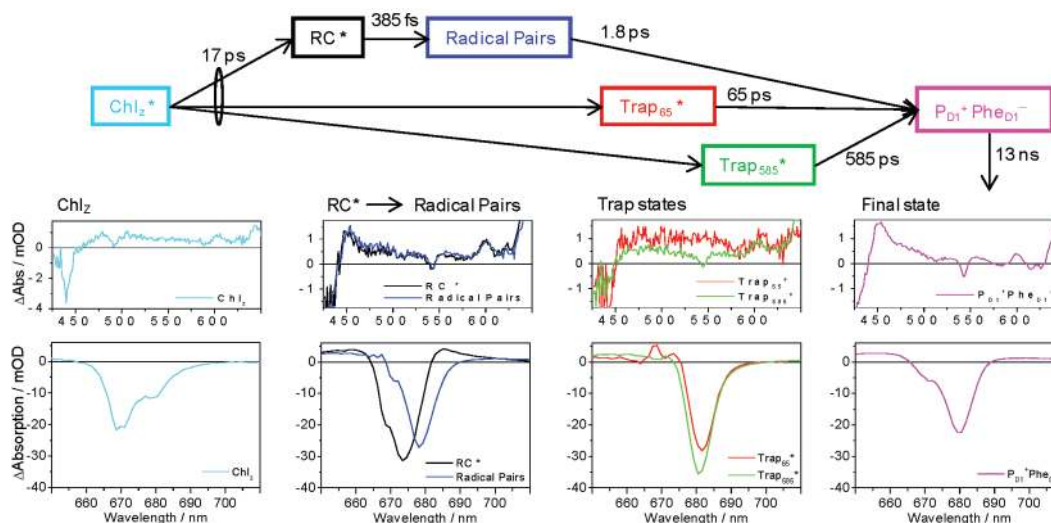
FIGURE 4: Simplified kinetic scheme with two trap states (top). SADS corresponding to the kinetic compartments for the 670 nm excitation data (bottom). All SADS are plotted on the same scale for better comparison (except for the 425−650 nm region for Chls$_z$).

respectively) (Figure S2 of the Supporting Information). As observed in the global analysis and the previous target analysis, additional RP2 is created on the 500 ps time scale, which is explained by the energy transfer from Trap$_{585}$. The SADS for the Chls$_z$ *, RC*, and mix of RP1s compartments have a spectral shape similar to that previously obtained (Figure 3). Due to photoselection, the bleach positions in the Q$_y$ absorption region are dependent on excitation wavelength. The Trap$_{65}$* SADS has Chl features with a bleach at 681.5 nm and SE at 690 nm but lacks features of Phe excited states. The Trap$_{585}$* SADS has a 681 nm bleach, SE at 690 nm, and a Phe Q$_x$ bleach but no Phe anion band, which indicates that Chl and Phe contribute to this excited state.

The initial distribution of excitation energy is wavelength dependent (Table S4 of the Supporting Information). For blue excitation (660, 662, 665, and 670 nm data sets linked), the initial excitation energy is distributed among the Chls$_z$ * (33%), RC* (43%), Trap$_{65}$* (14%), and Trap$_{585}$* (10%) states. After the transfer of energy from the Chls$_z$ to the RC core, 59% of the final charge-separated state (P$_{D1}$$^+Phe_{D1}$$^-$) is formed via RC*, 15% via Trap$_{65}$*, and 26% via Trap$_{585}$*. For red excitation (680, 682, and 685 nm data sets linked), an expected difference with respect to the blue data is found in the initial distribution of excitation energy: 60% is absorbed by RC*, 20% is trapped by Trap$_{65}$*, and 20% is trapped by Trap$_{585}$*. This indicates that both trap states arise from the central RC core pigments and not from the slow energy transfer from a red Chl$_z$.

DISCUSSION

Trap States. The presence of trap states in the PSII RC from higher plants at 4 K has been reported previously [a Chl trap (*37*) and a Phe trap (*38*)]. Here, at 77 K, two slow phases of charge separation, 65 and 585 ps, have been identified as originating from trap states with Chl and ChlPhe contribution, designated Trap$_{65}$ and Trap$_{585}$, respectively. The high-resolution fluorescence line narrowing (FLN) technique showed that there is a pronounced similarity between the spectroscopic features of the emitting and charge separating states in the PSII RC (*20*); therefore, and according to the spectral features (Figure 4), we conclude that Trap$_{585}$ originates from (Chl$_{D1}$Phe$_{D1}$)* and Trap$_{65}$ from (P$_{D1}$P$_{D2}$Chl$_{D1}$)*. In line with the idea of a distribution of

free energy difference around zero for charge separation (*38, 39*) and taking into account the disorder, it is reasonable to consider that charge separation may be activated in part of the RC complexes at low temperatures, leading to the observed slow kinetics. It is interesting to note that the excited states (Chl$_{D1}$Phe$_{D1}$)* and (P$_{D1}$P$_{D2}$Chl$_{D1}$)* can give rise to charge separation in either an activated or activation-less manner. This has been demonstrated by the two complementary target analyses. In the first target analysis, we concentrate on resolving the two parallel activation-less charge separation pathways on the fast, picosecond time scale (Figure 3). However, in this target analysis, the SADS of the penultimate state that rises with ≈50 ps and decays with ≈500 ps still contains chlorine excited-state absorption. These slow processes could well be interpreted as activated different pathways with the simplified target analysis (Figure 4). Here we need to compromise the fast phases to resolve the slow phases of charge separation present in the data, which explains why the time scales of the RC* → RP1 → RP2 evolution in the simplified target analysis are different from the ones found with the first target analysis.

Multiple Pathways of Charge Separation. The slow phase of Phe$_{D1}$$^-$ formation, present in the Q$_x$ and anion bands, was predicted by the model (*19, 40*) via the (P$_{D1}$P$_{D2}$Chl$_{D1}$Phe$_{D1}$)* → P$_{D2}$$^+P_{D1}$$^-$ → P$_{D1}$$^+Chl_{D1}$$^-$ → P$_{D1}$$^+Phe_{D1}$$^-$ mechanism. The first step excited state → radical pair is ultrafast, and it is not resolved in our target analysis. In line with the multimer model, in which the similarity in magnitude of the exciton coupling and energetic disorder results in exciton states delocalized over several cofactors (*14, 37*), it is reasonable to consider that depending on protein conformation, distinct exciton states are present in the system. Each of these leads to a different pathway of charge separation, which has also been demonstrated for the bacterial reaction center (*7−9*). At this point a question arises: is the protein actively involved in the determination of a pathway or is this determination only dependent on random static disorder? We suggest that at room temperature both pathways are possible. In case of a deterministic pathway, a single RC could switch between different states, which has also been observed for bacterial and plant light-harvesting complexes (*41−43*) providing functional flexibility. In the case of random disorder, the presence of two different charge separation pathways may help in the
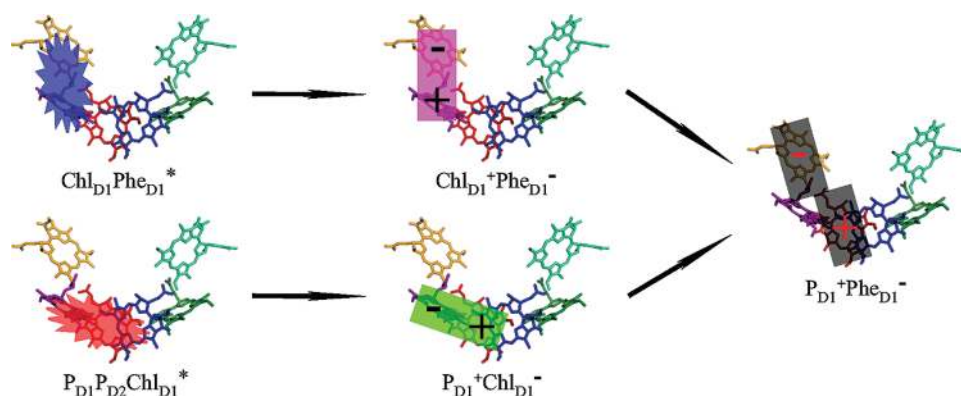
FIGURE 5: Excitation energy distribution in the excited state and charge separation events in the core of the PSII RC upon excitation in the Q_y absorption band (pigment arrangement from ref *13*). The excited states are represented as stars, and the radical pairs are represented as rectangles.

maintenance of high quantum efficiency in spite of the large disorder induced by the thermal energy at physiological temperatures.

The functional role of the protein matrix has been investigated before: changes in locally flexible domains in type I and II reaction centers have been shown to provide the means for adaptation of the enzyme to the ambient temperature (*44*), in the photsystem I complex of cyanobacteria protein dynamics have been shown to induce variation in energy transfer pathways (*45*), and for the bacterial reaction center the role of the protein matrix in controlling the kinetics of initial electron transfer has been demonstrated (*46*). In the latter contribution, the authors argue that the charge separation kinetics is determined by protein conformational changes induced by the absorption of light. In our view, the protein is inhomogeneously distributed prior to light absorption, and the slow protein motions are responsible for the presence of different pathways of charge separation.

In conclusion, two different charge separation pathways have been identified in the PSII RC from higher plants. Figure 5 shows the excitation energy distribution in the excited state and the charge separation events in the core of the photosystem II reaction center. Depending on protein configuration, the charge separation events follow the Chl_{D1} path (($Chl_{D1}P_{D1}P_{D2}$)* → $Chl_{D1}^+Phe_{D1}^-$ → $P_{D1}^+Phe_{D1}^-$) or the P_{D1} path (($P_{D1}Chl_{D1}$)* → $P_{D1}^+Chl_{D1}^-$ → $P_{D1}^+Phe_{D1}^-$). Therefore, Phe_{D1} is an electron acceptor, P_{D1} is an electron donor, and Chl_{D1} can act both as an electron donor and as an acceptor.

The capacity of the protein to fine-tune the energy of the excited states could be an advantage under stress conditions in which a modification of the kinetics of charge separation is required. This functional flexibility may be a key aspect in the successful performance of the PSII RC.

SUPPORTING INFORMATION AVAILABLE

Figures S1 and S2 and Tables S1−S4. This material is available free of charge via the Internet at http://pubs.acs.org.

REFERENCES

1. Kirmaier, C., Holten, D., and Parson, W. W. (1985) Picosecond-photodichroism studies of the transient states in *Rhodopseudomonas sphaeroides* reaction centers at 5K. Effects of electron transfer on the six bacteriochlorin pigments. *Biochim. Biophys. Acta 810*, 49–61.

2. Lockhart, D. J., Kirmaier, C., Holten, D., and Boxer, S. G. (1990) Electric field effects on the initial electron-transfer kinetics in bacterial photosynthetic reaction centers. *J. Phys. Chem. 94*, 6987–6995.

3. Steffen, M. A., Lao, K., and Boxer, S. G. (1994) Dielectric asymmetry in the photosynthetic reaction center. *Science 264*, 810–816.

4. Diner, B. A., and Rappaport, F. (2002) Structure, dynamics, and energetics of the primary photochemistry of photosystem II of oxygenic photosynthesis. *Annu. Rev. Plant Biol. 53*, 551–580.

5. Zinth, W., and Wachtveitl, J. (2005) The first picoseconds in bacterial photosynthesis: Ultrafast electron transfer for the efficient conversion of light energy. *ChemPhysChem 6*, 871–880.

6. Yeates, T. O., Komiya, H., Chirino, A., Rees, D. C., Allen, J. P., and Feher, G. (1988) Structure of the reaction center from *Rhodobacter sphaeroides* R-26 and 2.4.1: Protein-cofactor (bacteriochlorophyll, bacteriopheophytin, and carotenoid) interactions. *Proc. Natl. Acad. Sci. U.S.A. 85*, 7993–7997.

7. van Brederode, M. E., Jones, M. R., van Mourik, F., van Stokkum, I. H. M., and van Grondelle, R. (1997) A new pathway for trans-membrane electron tranfer in photosynthetic reaction centers of *Rhodobacter sphaeroides* not involving the excited special pair. *Biochemistry 36*, 6855–6861.

8. van Brederode, M. E., and van Grondelle, R. (1999) New and unexpected routes for ultrafast electron transfer in photosynthetic reaction centers. *FEBS Lett. 455*, 1–7.

9. van Brederode, M. E., van Mourik, F., van Stokkum, I. H. M., Jones, M. R., and van Grondelle, R. (1999) Multiple pathways for ultrafast transduction of light energy in the photosynthetic reaction center of *Rhodobacter sphaeroides*. *Proc. Natl. Acad. Sci. U.S.A. 96*, 2054–2059.

10. Zouni, A., Witt, H. T., Kern, J., Fromme, P., Krauss, N., Saenger, W., and Orth, P. (2001) Crystal structure of photosystem II from *Synechococcus elongatus* at 3.8 Å resolution. *Nature 409*, 739–743.

11. Ferreira, K. N., Iverson, T. M., Maghlaoui, K., Barber, J., and Iwata, S. (2004) Architecture of the photosynthetic oxygen-evolving center. *Nature 303*, 1831–1838.

12. Loll, B., Kern, J., Saenger, W., Zouni, A., and Biesiadka, J. (2005) Towards complete cofactor arrangement in the 3.0 Å resolution structure of photosystem II. *Nature 438*, 1040–1044.

13. Guskov, A., Kern, J., Gabdulkhakov, A., Broser, M., Zouni, A., and Saenger, W. (2009) Cyanobacterial photosystem II at 2.9-Å resolution and the role of quinones, lipids, channels and chloride. *Nat. Struct. Mol. Biol. 16*, 334–342.

14. Durrant, J. R., Klug, D. R., Kwa, S. L. S., van Grondelle, R., Porter, G., and Dekker, J. P. (1995) A multimer model for P680, the primary electron donor of photosystem II. *Proc. Natl. Acad. Sci. U.S.A. 92*, 4798–4802.

15. Dekker, J. P., and van Grondelle, R. (2000) Primary charge separation in photosystem II. *Photosynth. Res. 63*, 195–208.

16. Rappaport, F., and Diner, B. A. (2008) Primary photochemistry and energetics leading to the oxidation of the $(Mn)_4Ca$ cluster and to the evolution of molecular oxygen in Photosystem II. *Coord. Chem. Rev. 252*, 259–272.

17. Groot, M.-L., Pawlowicz, N. P., van Wilderen, L. J. G. W., Breton, J., van Stokkum, I. H. M., and van Grondelle, R. (2005) Initial electron donor and acceptor in isolated photosystem II reaction centers identified with femtosecond mid-IR spectroscopy. *Proc. Natl. Acad. Sci. U.S.A. 102*, 13087–13092.

18. Holzwarth, A. R., Müller, M. G., Reus, M., Nowaczyk, M., Sander, J., and Rögner, M. (2006) Kinetics and mechanism of electron transfer in intact photosystem II and in the isolated reaction center: Pheophytin

is the primary electron acceptor. *Proc. Natl. Acad. Sci. U.S.A. 103*, 6895–6900.

19. Novoderezhkin, V. I., Dekker, J. P., and van Grondelle, R. (2007) Mixing of exciton and charge transfer states in Photosystem II reaction centers: Modeling of Stark spectra with Modified Redfield Theory. *Biophys. J. 93*, 1293–1311.

20. Peterman, E. J. G., van Amerongen, H., van Grondelle, R., and Dekker, J. P. (1998) The nature of the excited state of the reaction center of photosystem II of green plants: A high-resolution fluorescence spectroscopy study. *Proc. Natl. Acad. Sci. U.S.A. 95*, 6128–6133.

21. Kwa, S. L. S., Newell, W. R., van Grondelle, R., and Dekker, J. P. (1992) The reaction center of photosystem II studied with polarized fluorescence spectroscopy. *Biochim. Biophys. Acta 1099*, 193–202.

22. van Stokkum, I. H. M., Larsen, D. S., and van Grondelle, R. (2004) Global and target analysis of time-resolved spectra. *Biochim. Biophys. Acta 1657*, 82–104.

23. Vacha, F., Joseph, D. M., Durrant, J. R., Telfer, A., Klug, D. R., Porter, G., and Barber, J. (1995) Photochemistry and spectroscopy of a five-Chlorophyll reaction center of Photosystem II isolated by using a Cu affinity column. *Proc. Natl. Acad. Sci. U.S.A. 92*, 2929–2933.

24. Eijckelhoff, C., Vacha, F., van Grondelle, R., Dekker, J. P., and Barber, J. (1997) Spectroscopic characterization of a 5 Chl *a* photosystem II reaction center complex. *Biochim. Biophys. Acta 1318*, 266–274.

25. Raszewski, G., Saenger, W., and Renger, T. (2005) Theory of optical spectra of Photosystem II reaction centers: Location of the triplet state and the identity of the primary electron donor. *Biophys. J. 88*, 986–998.

26. Germano, M., Shkuropatov, A. Y., Permentier, H., Khatypov, R. A., Shuvalov, V. A., Hoff, J. A., and van Gorkom, H. J. (2000) Selective replacement of the active and inactive pheophytin in reaction centers of photosystem II by 13^1-deoxo-13^1-hydroxy-pheophytin *a* and comparision of their 6 K absorption spectra. *Photosynth. Res. 64*, 189–198.

27. Diner, B. A., Schlodder, E., Nixon, P. J., Coleman, W. J., Rappaport, F., Lavergne, J., Vermaas, W. F. J., and Chisholm, D. A. (2001) Site-directed mutations at D_1-His198 and D_2-His197 of photosystem II in *Synechocystis* PCC 6803: Sites of primary charge separation and cation triplet stabilization. *Biochemistry 40*, 9265–9281.

28. Kamlowski, A., Frankemoller, L., van der Est, A., Stehlik, D., and Holzwarth, A. R. (1996) Evidence for delocalization of the triplet state ^{3}P680 in the D_1-D_2-cyt-b_{559} reaction center complex of photosystem II. *Ber. Bunsen-Ges. 100*, 2045–2051.

29. Noguchi, T., Inoue, Y., and Satoh, K. (1993) FT-IR studies on the triplet state of P680 in the Photosystem II reaction center: Triplet equilibrium within a chlorophyll dimer. *Biochemistry 32*, 7186–7195.

30. Raszewski, G., Diner, B. A., Schlodder, E., and Renger, T. (2008) Spectroscopic properties of reaction center pigments in Photosystem II core complexes: Revision of the multimer model. *Biophys. J. 95*, 105–119.

31. van Mieghem, F. J. E., Satoh, K., and Rutherford, A. W. (1991) A chlorophyll tilted 30° relative to the membrane in the Photosystem II reaction center. *Biochim. Biophys. Acta 1058*, 379–385.

32. Greenfield, S. R., Seibert, M., Govindjee, and Wasielewski, M. R. (1997) Direct measurement of the effective rate constant for primary charge separation in isolated photosystem II reaction centers. *J. Phys. Chem. B 101*, 2251–2255.

33. Greenfield, S. R., Seibert, M., and Wasielewski, M. R. (1999) Time-resolved absorption changes of the pheophytin Q_x band in isolated photosystem II reaction centers at 7 K: Energy transfer and charge separation. *J. Phys. Chem. B 103*, 8364–8374.

34. Schelvis, J. P. M., van Noort, P. I., Aartsma, T. J., and van Gorkom, H. J. (1994) Energy transfer, charge separation and pigment arrangement in the reaction center of photosystem II. *Biochim. Biophys. Acta 1184*, 242–250.

35. Rech, T., Durrant, J. R., Joseph, D. M., Barber, J., Porter, G., and Klug, D. R. (1994) Does slow energy transfer limit the observed time constant for radical pair formation in photosystem II reaction centers? *Biochemistry 33*, 14768–14774.

36. Wang, J., Gosztola, D., Ruffle, S. V., Hemann, C., Seibert, M., Wasielewski, M. R., Hille, R., Gustafson, T. L., and Sayre, R. T. (2002) Functional assymetry of photosystem II D1 and D2 peripheral chlorophyll mutants of *Chlamydomonas reinhardtii*. *Proc. Natl. Acad. Sci. U.S.A. 99*, 4091–4096.

37. Kwa, S. L. S., Eijckelhoff, C., van Grondelle, R., and Dekker, J. P. (1994) Site-selection spectroscopy of the reaction center complex of Photosystem II. 1. Triplet-minus-singlet absorption difference: Search for a second exciton band of P-680. *J. Phys. Chem. 98*, 7702–7711.

38. Groot, M. L., Dekker, J. P., van Grondelle, R., den Hartog, F. T. H., and Volker, S. (1996) Energy transfer and trapping in isolated photosystem II reaction centers of green plants at low temperature. A study by spectral hole burning. *J. Phys. Chem. 100*, 11488–11495.

39. Konermann, L., Gatzen, G., and Holzwarth, A. R. (1997) Primary processes and structure of the photosystem II reaction center. 5. Modeling of the fluorescence kinetics of the D_1-D_2-cyt-b_{559} complex at 77 K. *J. Phys. Chem. B 101*, 2933–2944.

40. Novoderezhkin, V. I., Andrizhiyevskaya, E. G., Dekker, J. P., and van Grondelle, R. (2005) Pathways and timescales of primary charge separation in the Photosystem II reaction center as revealed by simultaneous fit of time-resolved fluorescence and transient absorption. *Biophys. J. 89*, 1464–1481.

41. Rutkauskas, D., Novoderezhkin, V., Cogdell, R. J., and van Grondelle, R. (2004) Fluorescence spectral fluctuations of single LH2 complexes from *Rhodopseudomonas acidophila* strain 10050. *Biochemistry 43*, 4431–4438.

42. Rutkauskas, D., Olsen, J., Gall, A., Cogdell, R. J., Neil Hunter, C., and van Grondelle, R. (2006) Comparative study of spectral flexibilities of bacterial light-harvesting complexes: Structural implications. *Biophys. J. 90*, 2463–2474.

43. Krüger, T. P. J., Novoderezhkin, V. I., Ilioaia, C., and van Grondelle, R. (2010) Fluorescence spectral dynamics of single LHCII trimers. *Biophys. J.* (in press).

44. Shlyk-Kerner, O., Samish, I., Kaftan, D., Holland, N., Sai, P. S. M., Kless, H., and Scherz, A. (2006) Protein flexibility acclimatizes photosynthetic energy conversion to the ambient temperature. *Nature 442*, 827–830.

45. Brecht, M., Radics, V., Nieder, J. B., and Bittl, R. (2009) Protein dynamics-induced variation of excitation energy transfer pathways. *Proc. Natl. Acad. Sci. U.S.A. 106*, 11857–11861.

46. Wang, H., Lin, S., Allen, J. P., Williams, J. C., Blankert, S., Laser, C., and Woodbury, N. W. (2007) Protein dynamics control the kinetics of initial electron transfer in photosynthesis. *Science 316*, 747–750.